SSRG International Journal of Electronics and Communication Engineering
ISSN: 2348-8549/ https://doi.org/10.14445/23488549/IJECE-V13I4P121

Volume 13 Issue 4, 254-264, April 2026

Original Article

Clinical Decision Support System for Diabetic Foot Ulcer Detection and Classification Model Using Fine-Grained Deep Transfer Learning Model

S. Saint Jesudoss[1], K. Suresh Joseph[2]

[1]*Department of CSE, Rajiv Gandhi College of Engineering and Technology, Puducherry, India.*
[2]*Department of Computer Science, Pondicherry University, Puducherry, India.*

[1]*Corresponding Author : saint.2k5@gmail.com*

Received: 17 January 2026 Revised: 17 February 2026 Accepted: 20 March 2026 Published: 30 April 2026

Abstract *- Diabetic Foot Ulcers (DFU) remain a significant health issue for diabetes patients, necessitating early and accurate detection for rapid intervention. Because of insufficient blood circulation, the reappearance of these ulcers can result in 84% of lower limb amputation and even lead to mortality. Severe diabetes risk patients need costly medications, routine check-ups, and appropriate personal cleanliness to avoid DFUs that affect 15–25% of diabetics. Early detection, accurate diagnosis, proper care, and rapid response can eliminate amputations and death rates by early and robust DFU detection from image analysis. Therefore, efficient DRC detection is a necessity for enhanced patient care. Recently, Deep Learning (DL) systems have attained substantial consideration in the prognosis and diagnosis of DFU detection through different medical imaging conditions. This study develops an Automated Diabetic Foot Ulcer Detection and Classification utilizing Snow Ablation Optimization with Deep Learning (ADFUDC-SAODL) approach. The ADFUDC-SAODL approach enables early detection and classification of DFU leveraging a fine-grained DL approach. In the ADFUDC-SAODL approach, the MResCaps-based feature extraction approach is employed. The MResCaps method is an enhancement of the Capsule Network (CapsNet), which comprises a convolutional layer, a Primary Capsule (PC) layer, and a Digit Capsule (DigitCaps) layer. As the CapsNet model makes use of a single convolution layer, fundamental features of the image are extracted. To extract detailed features and enhance the classification efficiency of the CapsNet method, residual blocks are utilized rather than the convolution layer. Besides, a Convolutional Recurrent Neural Network (CRNN) approach was performed for the classification of DFU. At last, the Snow Ablation Optimization (SAO) method adjusts the hyperparameter values of the CRNN method optimally and leads to enhanced classification performance. An extensive set of simulations was involved to exhibit the encouraging outcomes of the ADFUDC-SAODL methodology. The simulated outcomes implied the proficient performance of the ADFUDC-SAODL methodology across other recent models.*

Keywords *- Deep Learning, Diabetic Foot Ulcer Detection, Snow Ablation Optimization, Image Pre-processing, Feature Extraction.*

1. Introduction

Diabetes is a long-term illness that has a massive negative impact on individuals' lives, people, and families globally [1]. The DFU is the primary difficulty causing diabetes that could cause lower-limb elimination. Routine foot check-ups by medical experts are necessary for patients with DFU growth that is frequently expensive and/or requires recommendations for professional treatment [2]. The study indicates that the healthcare facilities that treat DFU were incapable of dealing with the rising percentage of patients owing to ineffectively trained health professionals, which is mainly common in low-income rural areas and countries [3]. Over the last ten years, the growth of information and digital technologies has empowered the formation of novel computer-based solutions for health care, including trauma care. Lower limb amputation can arise as a result of deficient macrovascular and microvascular tissue infection and perfusion. A diabetic patient with a higher threat of foot needs standard clinician visits, enduring costly treatment, and hygienic self-care for preventing additional difficulties [4]. It imposes extreme financial trouble on the patients and their families, mainly in underdeveloped countries, whereas the expenditure on medication for this disease is higher. The capability to rapidly interfere and obtain a suitable treatment to both stop the development of amputation and heal foot ulcers is made possible by the initial recognition and healthier classification of foot troubles [5]. Initial observation by self-examination at home might be beneficial in inhibiting the start and

development of DFU. Initial DFU recognition and medication will induce a high survival rate and, eventually, a low death rate [6].

A whole investigation of healthcare data is required for experts to initiate a precise identification for DFU recognition [7]. Classical methodologies are labor-intensive and prone to human errors. The usage of computer-aided diagnosis techniques reduces prices while improving execution. Current improvements in mobile and comfortable healthcare gadgets can aid in monitoring diabetes and its significance by prolonged healing and amplifying the living standards for patients by detecting and monitoring damaging foot stress and infection [8]. Sensors are tools that recognize biological, physical, and chemical signs and provide a mechanism for measuring and recording these signs.

Various industrialized sensor technologies have medical benefits. While the new sensor and sensor-dependent mechanical methods were tested, non-medical fields will modify them for usage in their manufacturing applications [9]. The development of novel-generation medicinal sensors recommends the prolonged usage of these devices within the medical industry.

In the current digital health care system, medical imaging is used to diagnose numerous patient difficulties [10]. The efficiency of conventional DL and Machine Learning (ML) classification techniques for addressing classification problems in medical imaging is intensely reliant on Feature Selection (FS), and representation models are sensitive to shapes, colors, and sizes.

This study develops an Automated Diabetic Foot Ulcer Detection and Classification utilizing Snow Ablation Optimization with Deep Learning (ADFUDC-SAODL) approach. The major intention of the proposed model is to exploit a hyperparameter-tuned DL model for the DFU detection process. The key contributions are listed as follows:

- An effective ADFUDC-SAODL method comprising pre-processing, MResCaps-based feature extraction, CRNN-based classification, and SAO-based hyperparameter tuning is developed for DFU detection. To the best of our knowledge, the presented model never existed in the literature.
- Designs a new MResCaps model for feature extraction, which utilizes the residual blocks to decrease the drawbacks of the CapsNet model to enable deeper spatial information and boost overall efficiency.
- Employ CRNN for the DFU detection and classification process, which helps to effectively capture spatial lesion characteristics and sequential contextual dependencies from medical images.
- Hyperparameter tuning using the SAO model for network training helps to enable optimal selection of hyperparameter values to enhance classification performance, convergence stability, and generalization.

2. Literature Survey

Murthy et al. [11] developed a novel pre-processing pipeline that depended on the Shades of Gray color constancy method. Utilizing the DFINET-AO model, features are saved later the database is divided and pre-processed. To understand the pathological and standard range of diabetes, numerical/text data and image data were divided autonomously. Patient's Foot images with abnormal diabetes exposure were divided together and categorized utilizing Pre-trained Fast CNN (PFCNNs) that were trained on the U++ network. The authors [12] recommended a reliable, precise, fast end-to-end conventional ML model. For extracting aspects unchanging to rotation, translation, and scaling transformation, the work used the SURF and SIFT approaches, which are united with the BOF system. The technique utilized various pre-proficient DL methods to associate ML methods trained with DL and personalized aspects. This study is new as no preceding researchers have utilized conventional ML methods for the DFU diagnosis from current images, nor have they utilized BOF, SIFT, or SURF methods. In [13], a new technique is presented for effective identification of DFU imageries. Primarily, a DFU dataset is created using multi-spectral DFU imagery, and pre-processing was completed with the help of an AMF. Subsequently, the image has been partitioned by the enhanced Fuzzy C–Means (FCM) PSO method. Later, a sum of 2nd-order statistical texture aspects containing contrast, correlation, and uniformity was created by the GLCM model.

Nagaraju et al. [14] propose a new SSO with DL-allowed DFU detection and classification (SSODL-DFUDC) model. The suggested model uses the InceptionResNetv2 method for feature vector creation to achieve this. Meanwhile, the error and trial physical parameter tunings of the InceptionResNetv2 method are an erroneous and tedious method; the SSO method is utilized for the optimum hyperparameter choice that sequentially improves the complete DFU classifier outcomes. Furthermore, the DFU classification occurs utilizing the Stacked Sparse Autoencoder (SSAE) method. Das et al. [15] proposed to advance an effective DL model for the initial categorization of ischemia in DFU.

Consequently, a new CNN structure (HCNNet) is presented by incorporating various hybridized blocks from dense, residual modules, and inception together with properly retained Squeeze-and-Excitation (SE) blocks and an intermediary transition layer. The presented HCNNet is trained numerous times utilizing numerous learning rates and optimizer settings to enhance its execution. Das et al. [16] proposed a model based on an effectual CNN technique. Consequently, a new CNN-based technique (AESPNet) was developed, where convolution layers were stacked on top of each other in an equivalent fashion and with transitional attention modules for executing DFU vs usual skin classifications. The AESPNet contains dual blocks, whereas changing-sized kernel convolutional layers were linked

equivalently for superior global and local feature abstraction. Almufadi et al. [17] propose an automatic technique for classifying and identifying DFU utilizing Transfer Learning (TL). DFU is generally classified into infection and ischemic conditions that are challenging to differentiate graphically. The research assesses the efficiency of pre-trained Deep CNN (DCNN) methods for independent DFU recognition. Moreover, the study presents E-DFu-Net, a new method that emerged from current structures, intended to alleviate overfitting.

Sait and Nagaraj [18] examine an innovative method for achieving strong and explainable DFU categorization. The presented DFUs identification combines MobileNet V3-SWIN and ensemble splines-based KAN with SHAP value by categorizing the severity of DFU into ischemia and infection classes. The authors [19] present the DFU_XAI model to amplify the intelligibility of DL techniques for the DFU model and ensure medical relevance. Gudivaka et al. [20] introduce the Advanced ML methodology for diabetic foot ulcer categorization. The categorization depends upon constant technological advancements, and the assistance of ML for utilization in DFU treatment is varied, including upgraded clinical decisions that depend upon Ulcer classification. The authors [21] present an innovative methodology for DFU classification by emerging and assessing both custom and established DL approaches. In [22], a stacked parallel convolution layer enabled CNN has been presented, called DFU MobileNet, by categorizing skin infested with DFU, as opposed to normal skin. Though several DFU detection models exist in the literature, there is a necessity for an automated DL model for enhanced detection performance. As hyperparameter values significantly influence the performance of the DL model, the manual trial and error process can be replaced using automated hyperparameter optimizers. Therefore, this study applies the SAO-based hyperparameter optimizer to tune the hyperparameter values of the DL architecture.

3. Proposed Framework

In this paper, a new ADFUDC-SAODL approach is introduced. The ADFUDC-SAODL approach allows the classification and detection of DFU disease images. It comprises four distinct stages involved in image pre-processing, MResCaps-based feature extractor, CRNN-based DFU detection, and SAO-based parameter selection. Figure 1 depicts the entire procedure of the ADFUDC-SAODL methodology.

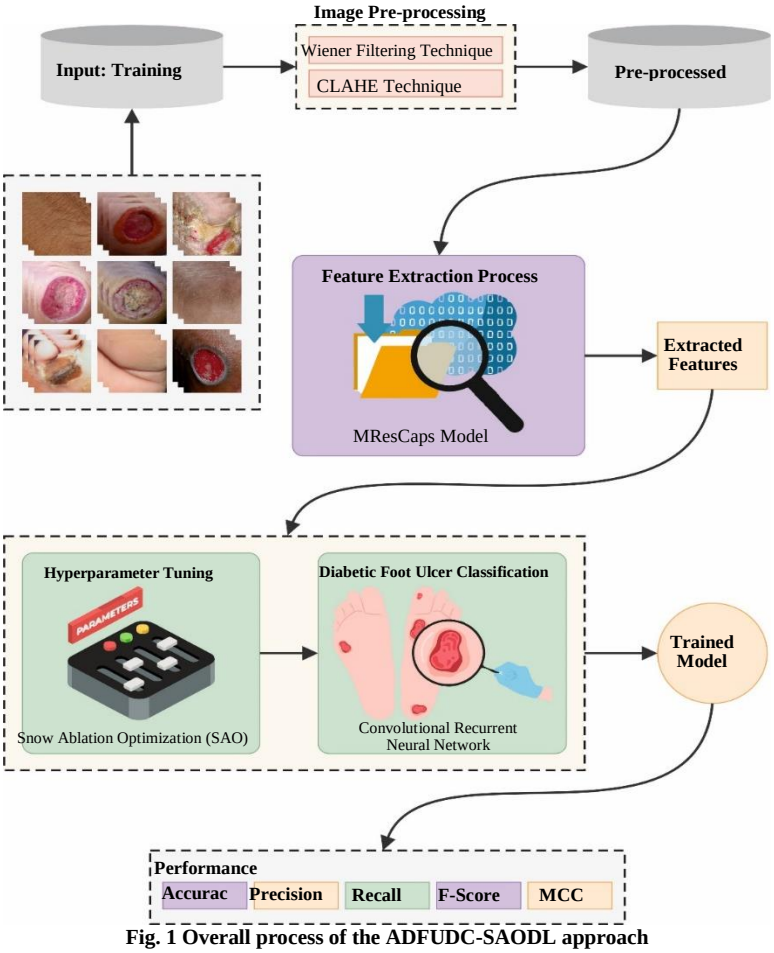

Fig. 1 Overall process of the ADFUDC-SAODL approach

3.1. Pre-Processing Pipeline

At first, the image pre-processing step involves dual levels, such as noise removal using the WF method and contrast enhancement using the CLAHE method. WF attains the finest equilibrium among noise smoothing and inverse filter [23]. It eliminates the additive noise while additionally inverting the blurring. It decreases the complete MSE throughout the process of noise smoothing and inverse filtering. WF estimates the original image linearly. A stochastic basis strengthens the model.

Based on the orthogonality idea, the WF in the Fourier domain is specified basically in the following.

$$W(f_1, f_2) = \frac{H * (f_1, f_2) S_{xx}(f_1, f_2)}{|H(f_1, f_2)|^2 S_{xx}(f_1, f_2) + S_{\eta\eta}(f_1, f_2)} \quad (1)$$

Now $S_{xx}(f_1, f_2)$ and $S(f_1, f_2)$ represent the power spectra of the additive noise, and the early image is the blur filter. The WF contains two different portions: a noise-smoothing part and an inverse filter. It not only deconvolves the signal by inverse filtering, but also decreases noise with a compression process.

CLAHE is utilized for improving the local contrast that is accessible in the image, transferring to the pixel degree distribution of every area [24]. Then, the homomorphic filtering method was utilized to enhance the image features with a reduction in the noise within the image. Similarly, the accuracy of the image texture using the feature particulars is gained, while devastating the improvement for noise. Near these images were obtained by developing many equal image grids, named the region dimension.

The regional architecture as regards the image is divided into 3 segments in the image corner marked as well as the corner region, the edges of this region are recorded by the border region, along with another portion within the center scored, and the interior region. The algorithm contains the ability to decrease the growth by cutting the histogram before, and the image contrast was improved. This CLAHE is used in smaller areas in the image in its position within the entire image, and then, the problem increases. This minor portion of an image is called a tile. The problem of significant contrast improvement is overcome by utilizing CLAHE, such as by providing an edge degree by the histogram. These limited values are termed the clip bounds that express the significant elevation of a histogram. Precisely how to calculate the clip boundary of histograms is said in Eq. (2).

$$B = M/N \left(1 + \frac{a}{100} Smax\right) \quad (2)$$

M represents the sum of pixels in each block, N denotes the dynamical range in these blocks, $Smax$ refers to maximal grades, and α represents the pin component.

3.2. Feature Extractor using MResCaps

Due to the process of feature extraction, the MResCaps method is exploited. The MResCaps structure is an improved variety of the conventional CapsNet architecture, containing a PC layer, a Digit Capsule (DigitCaps) layer, and a convolutional layer [25]. Meanwhile, the CapsNet structure utilizes a solitary convolution layer, and more essential features of the image are removed. To describe these features and enhance the classification performance of the CapsNet structure, residual blocks are utilized rather than the convolution layer. Primarily, a model stimulated by the ResCaps methods, which uses a solitary residual block, is generated.

Next, the ResCaps method, a model containing three equivalent ResCaps, is introduced by improving the lane counts. This method was called 3ResCaps. Formerly, residual blocks were included in the 2nd and 3rd lanes to attain features with various particulars in every lane. Whereas dual residual blocks are applied in the 2nd lane, 3 residual blocks were employed in the 3rd lane. During this initial lane 1, a residual block was applied, accompanied by dual consecutive residual blocks in the next lane, and 3 consecutive residual blocks in the last lane. The usage of residual blocks in every lane and the upsurge in the number of convolution operations allowed more features to be removed in every lane. Whereas more surface features were attained in the initial lane, more comprehensive features were gained in the succeeding lanes. Hence, initial capsules with various features were made in every lane. These initial capsules are then routed and concatenated to the output values, and the digit capsule layer is acquired by utilizing a dynamic routing model.

3.2.1. Residual Block Unit

While the layer counts improved in the structure, the training set achieved saturation more rapidly, resulting in a decrease in performance. To tackle this problem, the ResNet model is proposed. The ResNet method contains residual blocks. It resolves the issue of explosion and gradient decrease in a deep network framework. It additionally enables deep network training and increases the classification precision of images. It utilizes skip connections for learning relationships between outputs and inputs.

3.2.2. CapsNet

CapsNet is a structure introduced that stores the entities in an image (sampling parameters like angle, orientation, position, pose) in capsules and presents vector outputs instead of scalar outputs in CNNs. Whereas in CNNs, the pooling layer guarantees that neurons have invariance of viewpoint, in CapsNet, neurons are substituted by capsules along with a relationship among the lower-level and the higher-level capsules presented by the dynamic routing model. Hence, the part-whole relationship is determined, and the pooling procedure is unnecessary.

Its framework contains a primary capsule, a digit capsule, and convolutional layers. Primary, the basic features of the image, after undertaking the convolutional course, are removed, and the feature mapping extraction is forwarded to the layer of the primary capsule.

Now, the features, once again exposed to the process of convolution, are separated into capsules over the process of reshaping. During this layer, the capsules penetrated the squash function and are assumed as input to the layer of the digit capsule. In said layer, the dynamical routing function is utilized, and the capsule with the highest possibility produces the output value. Then, image reconstruction was carried out over the loss calculation.

3.2.3. Dynamic Routing Model

This model is a technique for matching low-level capsules with high-level capsules. The primary capsule layer outputs are distributed to the digit capsule layer, penetrate the dynamic routing algorithm, and the output values are considered. The output values from the capsules (u) were decided by multiplying them with the weight matrix (W_{ij}), demonstrating the projected output value of every capsule $\left(\hat{u}_{j|i}\right)$ in Eq. (3). Here, i denotes low-level layer capsules, and j represents high-level layer capsules.

$$\hat{u}_{j|i} = W_{ij} u_i \tag{3}$$

The primary value of the short-term correspondence variable is represented as b_{ij} is set to 0. The matching coefficient value c_{ij} is gained by passing b_{ij} over the softmax function in Eq. (4). The weighted sum s_j is achieved by taking the matching coefficient sum and the predictable output value, Eq. (5). The capsule's output value v_j is decided by passing the value s_j over the squashing function Eq. (6). The loop ends by upgrading the value b_{ij}, with its primary value being 0 Eq. (6).

$$c_{ij} = \frac{\exp\left(b_{ij}\right)}{\sum_k \exp\left(b_{ik}\right)} \tag{4}$$

$$s_j = \sum_i c_{ij}\, \hat{u}_{j|i} \tag{5}$$

$$v_j = \frac{\|s_j\|^2}{1 + \|s_j\|^2} \cdot \frac{s_j}{\|s_j\|} \tag{6}$$

$$b_{ij} = b_{ij} + \hat{u}_{j|i} v_{ij} \tag{7}$$

The squash function presents vector outputs with likelihood values in the interval of (0-1), representing the existence probability inside the capsule. The initial portion of the squash function scales the values to the range of (0-1); however, the next portion carries out the conversion to a unit vector. The function is provided in Eq. (8).

$$v_j = \frac{\|s_j\|^2}{1 + \|s_j\|^2} \frac{s_j}{\|s_j\|}. \tag{8}$$

Here, s_j refers to a weighted sum of the low-level capsule, and v_j denotes the capsule output value.

$$L_k = T_k \max(0, m^+ - \|v_k\|)^2 + \lambda(1 - T_k)\max(0, \|v_k\| - m^-)^2. \tag{9}$$

When there is a class k within an equation, Tk $= 1$, or else Tk $= 0$.

3.3. Classification using the CRNN Model

Besides, the CRNN methodology is performed for the DFU classification. The presented CRNN method comprises hidden layer (HL) output and input layers that have the responsibility to accept as input, removing the P- and S-arrivals features, and allowing the evaluation and expression of P- and S- arrivals, correspondingly [26].

3.3.1. Input Layer

The inputs of the CRNN method were unique, taking into consideration that DL techniques have a strong capability of feature extraction. The requirement for added transformation or filtering is unnecessary, which could affect the real-time implementation. The maximal total scaling model is applied to linearly scale in the interval of [−1, 1] to remove the impact of amplitude transformations:

$$X' = \frac{X}{\max[abs(X)]} \tag{10}$$

Whereas X' represents a standardized input waveform, X denotes a unique waveform of input, max(·) refers to the outcomes of argument's maximal value, and abs implies the outcome of argument's absolute value.

3.3.2. HL

The HLs represent fundamentals in the CRNN method. Three new layers, such as the LTF, the interpretation, and the STF layers, are calculated to flawlessly remove the P- and S-arrivals features. The layer of STF utilizes a convolutional layer to remove, whereas the pooling layer has been used to keep the length uniformity of the outputs and inputs. The intricacy channels (n) and intricacy kernel width (l) are either significant parameters that influence the STF representations, or their value are decided over orthogonal examinations. The convolutional layer's calculation process is described as follows.

$$c_t^i = ReLU(X' * K^i + b^i) = \max\left(0, \sum_l X'_{t+l}\, k_l^i + b^i\right) \tag{11}$$

Here, c_r^i means tth output from the ith convolution layer, and $c_f = [c_t^1\ c_t^2\ \ldots\ c_t^n]$; $ReLU(\cdot)$ represents rectified linear

unit; $*$ denotes convolution operation; K^i refers to ith convolution kernel with length l, and b^i symbolize ith bias. This LTF layer utilizes a GRU, which is a representation architecture of an RNN. The GRU employs resetting and updating gates by comprehending information updating and forgetting, and utilizes state vectors (h_t) to save previous data before every sampling point, hence, understanding the LTF extraction by a smaller computation amount. The h_f size is defined through the GRU components (m), which is additionally decided over orthogonal examinations.

$$h_t^i = u_{t-1}^i h_{t-1}^i + \left(1 - u_{t-1}^i\right)\tanh\left(\sum_i W^{i,j} r_{t-1}^j \mathrm{h}_{\mathrm{t-1}}^{\mathrm{j}} + \sum_i U^{i,j}\, c_t^j\right) \quad (12)$$

Now, h_r^i refers to tth output from the ith GRU unit, and $h_f = [h_t^1 h_t^2 \ldots h_t^m]$; u_t^i and r_t^i characterize the tth values from the ith reset and update gate, correspondingly; tanh implies hyperbolic tangent; $W^{i,j}$ and $U^{i,j}$ represent the weight of historic data and present input, correspondingly.

The explanation layer overapplies a convolution layer to handle the feature gained within the layer of LTF. On one side, h_t is compressed within a 3-D vector $a_t = [a_t^N\ a_t^P\ a_t^s]^T$ to enable the following processing in the outcome layer, whereas a_t^P, a_t^N, and a_t^S denote P-arrival, non-arrival, and S-arrival features, individually, parallel to the t_{th} sample point. Conversely, the local networks of the convolution layer could examine the LTF local fluctuations, increasing the P- and S-arrivals accuracy selection. To improve the simplification capability of the CRNN method, the function of dropout is included in every HL, which restrains overfitting by arbitrarily dropping components in the training procedure.

3.3.3. Output Layer

Meanwhile, the interpretation layer outputs vary from zero to positive infinities; an absence of contrast between the post- and pre-sample points. This softmax classifier standardizes the outputs of the interpretable layer to a likelihood matrix $p_t = [p_t^N\ p_t^P\ p_t^s]^T$:

$$p_t^{\mathrm{k}} = \frac{e^{a_t^k}}{\sum_{i=1}^3 e^{a_t^i}} \quad (13)$$

Whereas p_t^{k} represents the predicted likelihood of the kth class on the tth waveform's sampling point, and k captures S, N, and P equivalent to S-, non-, P-, and arrival, corresponding.

3.4. SAO-based Parameter Tuning

At last, the SAO model alters the parameter values of the CRNN approach optimally, resulting in a greater classification outcome. Snow is the utmost attractive wonder within nature, particularly in winter [27]. Snow melt plays a critical part in environments, affecting the growth of crops and human well-being. From an actual perception, snow could convert into liquid water. This contains dual main physical procedures: sublimation and melting. Also, the melted liquid could additionally be evaporated into vapor. The SAO illustrates stimulation from the melting methods of snow and sublimation in natural ecosystems.

3.5. Population Initialization

The SAO iterative method initiates with an arbitrarily created population. It is denoted as a matrix $of\ N \times Dim$.

$$Z = \begin{bmatrix} z_{1,1} & z_{1,2} & \cdots & z_{1,Dim-1} & z_{1,Dim} \\ z_{1,2} & z_{2,2} & \cdots & z_{2,Dim-1} & z_{2,Dim} \\ \vdots & \vdots & \vdots & \vdots & \vdots \\ z_{N-1,1} & z_{N-1,2} & \cdots & z_{N-1,Dim-1} & z_{N-1,Dim} \\ z_{N,1} & z_{N,2} & \cdots & z_{N,Dim-1} & z_{N,Dim} \end{bmatrix}_{N \times Dim} \quad 14)$$

whereas N signifies the size of the population and Dim represents the dimension.

3.5.1. Exploration Stage

The exploration tactic creates the principle of SAO. This unbalanced movement happens as liquid or snow water changes to vapor, causing an excellent distribution of the hunters. This occurrence is denoted by Brownian motion, a stochastic method that is extensively used to pattern stock price fluctuations, animal foraging, and particle movement, among other applications. The typical Brownian motion step size is directed by standard distributions, through a variance of one and a mean of zero, as specified in Eq. (15):

$$RB(Dim) = \frac{1}{\sqrt{2\pi}} \exp\left(-\frac{\chi^2}{2}\right) \quad (15)$$

Over uniform and dynamic step sizes, Brownian motion discovers the possible region representing the dispersion of vapor within the search spaces. So, position upgrade formulation in the process of exploration is provided by Eq. (16).

$$Z_i(b+1) = Elite(b) + RB(Dim) \times \left(\theta_1 \times \left(G(b) - Z_i(b)\right) + (1-\theta_1) \times \left(\overline{Z}(b) - Z_i(b)\right)\right) \quad (16)$$

whereas $Z_i(b)$ signifies the agent i inside the iteration b, $RB(Dim)$ means the Brownian motion, and θ_1 represents the amount selected at random from [0,1]. Furthermore, $G(b)$ mentions the present finest solution, $Elite(b)$ denotes an individual selected randomly from the group elite, and $\overline{Z}(b)$ states the centeral location.

$$\overline{Z}(b) = \frac{1}{N}\sum_{i=1}^{N} Z_i\,(b) \quad (17)$$

$$Elite(b) \in [G(b), Z_{2nd}(b), Z_{3rd}(b), Z_c(b)] \quad (18)$$

whereas $Z_{2nd}(b)$ and $Z_{3rd}(b)$ represents the 2nd and 3rd of the present population individuals. $Z_c(b)$ signifies the topmost 50 percent of individual suitability values, computed by utilizing Eq. (19).

$$Z_c(b) = \frac{1}{N_1}\sum_{i=1}^{N_1} Z_i\,(b) \tag{19}$$

whereas N_1 indicates the leader counts, which are proportional to the group size. $Z_i(b)$ displays the ith best leader. In every iteration, $Elite(b)$ is arbitrarily chosen from a set encompassing the present finest outcome, the 2nd and 3rd finest individuals, and the leader center location.

3.5.2. Exploitation Stage

With the SAO model, the exploitation aspects were underlined. If the snow melts to liquid, the searching agents were stimulated to focus on using higher-feature outcomes in the existing optimal. This formulation is stated in Eq. (20) below.

$$Z_i(b+1) = M \times G(b) + RB(Dim) \times \left(\theta_2 \times \left(G(b) - Z_i(b)\right) + (1-\theta_2) \times \left(\overline{Z}(b) - Z_i(b)\right)\right) \tag{20}$$

whereas M represents the melting rate of snow, θ_2 means a number arbitrarily chosen from the $[-1,1]$ range to improve communication among individuals. During these methods, with the aid of the dual cross term $\theta_2 \times \left(G(b) - Z_i(b)\right)$ and $(1-\theta_2) \times \left(\overline{Z}(b) - Z_i(b)\right)$, individuals were persuaded to utilize the group center information and present optimum solutions to improve possibly valued areas.

$$M = \left(0.35 + 0.25 \times \frac{e^{\frac{b}{b_{max}}} - 1}{e-1}\right) \times T(b), T(b) = e^{\frac{-b}{b_{max}}} \tag{21}$$

Whereas $T(b)$ denotes the present temperature, b_{max} signifies the maximal amount of iteration, and b represents the present amount of iteration.

3.5.3. Dual-Population Module

A two-group framework is developed by representing the method of alteration from snow to liquid to vapor, demonstrating the exploitation and exploration behaviors of individuals within the solution outcome. During the primary phase, the method arbitrarily distributes every individual into dual, equivalently sized subdivisions, each of which is liable for exploitation and exploration, correspondingly. In the process of iteration, the dimension of the exploration cluster progressively rises. In contrast, the exploitation group size lessens, respectively, modifies, and pretends the change in individual performance from central exploitation to widespread exploration. The pseudocode of the SAO model is displayed in Algorithm 1.

Algorithm 1: Pseudocode of the SAO model

```
Start
Initializing relevant parameter
        Utilizing Eq. (14), set the population
While b < b_max + 1
        Compute M by utilizing Eq. (21)
        for every agent
          Exploration stage: Upgrading individual
location by Eq. (16)
          Exploitation stage: Upgrading individual
location by (20)
        end for
        Fitness assessment
        Upgrading G(b)
        b = b + 1
end while
End
```

The SAO model explains how an FF can reach an increased execution of the classifier. It specifies a positive integer to indicate the superior accomplishment of candidate performances.

$$fitness(x_i) = Classifier\_Error\_Rate(x_i) = \frac{No.of\ misclassified\ instances}{Total\ no.of\ instances} \times 100 \tag{22}$$

4. Performance Assessment

In this work, the experimental examination of the ADFUDC-SAODL system is verified under the DFU database [28]. The database contains 1000 samples under dual classes defined in Table 1. Figure 2 represents the sampled images.

Table 1. Dataset Details

Classes	No. of Samples
Normal (Healthy)	500 samples
Abnormal (DFU)	500 samples
Total Samples	**1000**

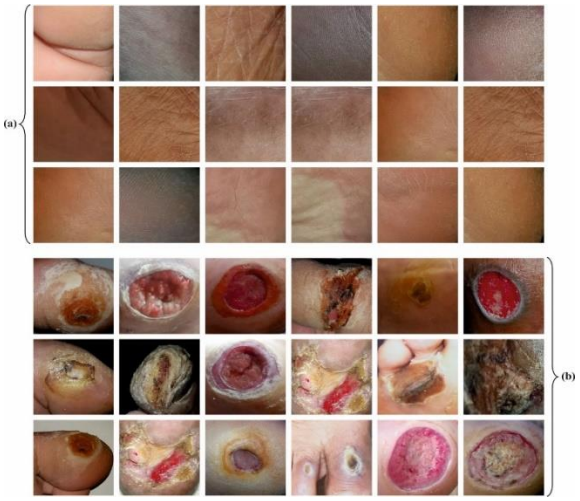

Fig. 2 Sample images (a) normal, and (b) abnormal.

Figure 3 implies the classification analysis of the ADFUDC-SAODL model below 80% and 20%. Figures 3a-3b portray the confusion matrices with accurate recognition of 2 classes. Figure 3c implies the PR examination, demonstrating the best performance across all 2 classes. Additionally, Figure 3d portrays the ROC examination, depicting effective outcomes with greater ROC analysis for the dissimilar classes.

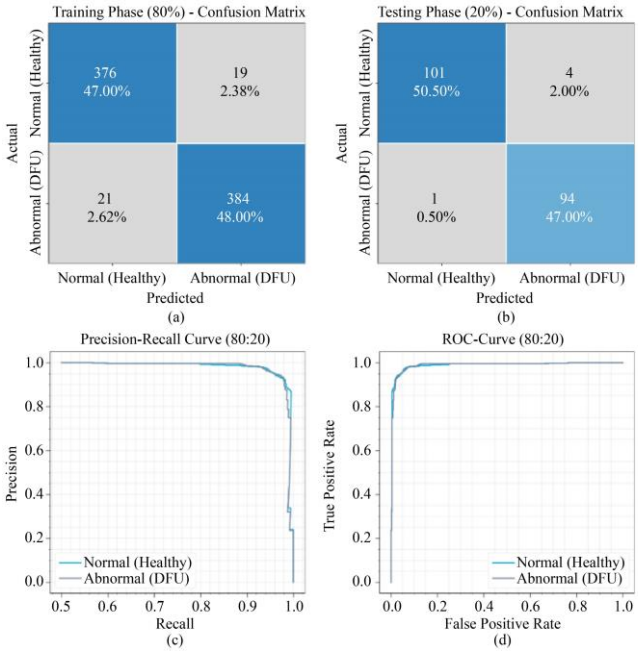

Fig. 3 Splits of 80 and 20 (a, b) confusion matrices, and (c, d) Graph of PR and ROC.

Table 2 and Figure 4 denote the DFU recognition analysis of the ADFUDC-SAODL system below 80%TRAPH and 20%TESPH. The solution implies that the ADFUDC-SAODL system correctly recognized the instances. With 80%TRAPH, the ADFUDC-SAODL methodology gains an average $accur_y$, $preci_n$, $recal_l$, F_{score} and MCC of 95.00%, 95.00%, 95.00%, 95.00%, and 90.00%, respectively. Also, on 20%TESPH, the ADFUDC-SAODL methodology presents an average $accur_y$, $preci_n$, $recal_l$, F_{score} and MCC of 97.57%, 97.47%, 97.57%, 97.50%, and 95.04%, respectively.

Table 2. DFU detection outcome of the ADFUDC-SAODL system with 80% and 20%

Class	$Accur_y$	$Preci_n$	$Recal_l$	F_{score}	MCC
80% TRAPH					
Normal (Healthy)	95.19	94.71	95.19	94.95	90.00
Abnormal (DFU)	94.81	95.29	94.81	95.05	90.00
Average	**95.00**	**95.00**	**95.00**	**95.00**	**90.00**
20% TESPH					
Normal (Healthy)	96.19	99.02	96.19	97.58	95.04
Abnormal (DFU)	98.95	95.92	98.95	97.41	95.04
Average	**97.57**	**97.47**	**97.57**	**97.50**	**95.04**

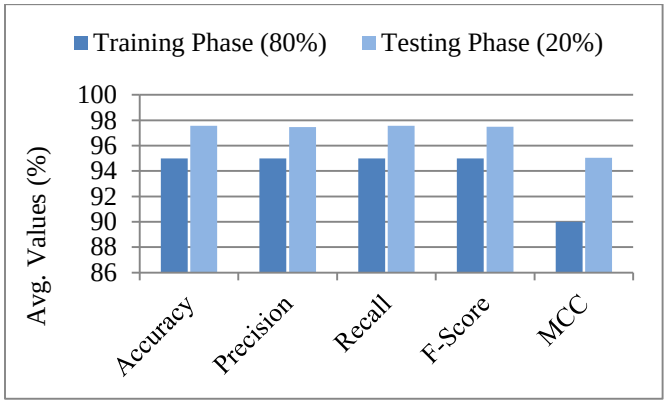

Fig. 4 Average of the ADFUDC-SAODL method at splits of 80 and 20

Figure 5 represents the classification outcomes of the ADFUDC-SAODL system below 70% and 30%. Figures 5a-5b define the confusion matrices with exact identification of 2 classes. Figure 5c exemplifies the PR curves, depicting the promising performances through 2 classes. Eventually, Figure 5d illustrates the ROC curve, implying trained solutions with better values of ROC for numerous classes.

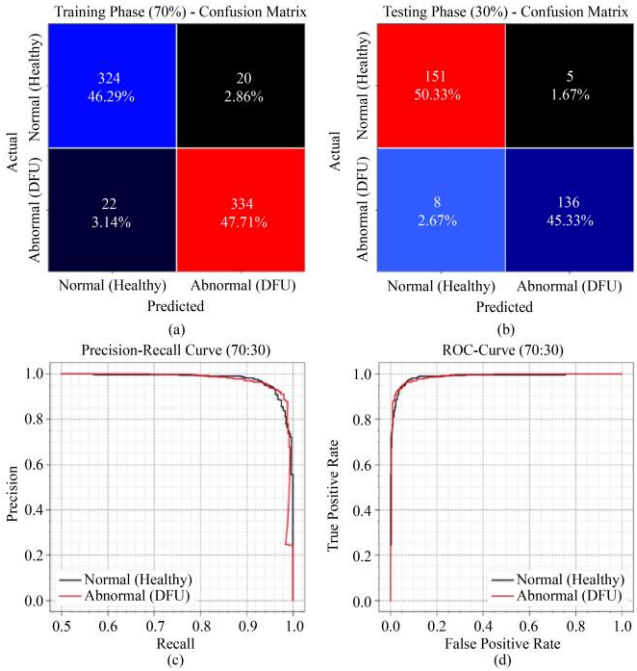

Fig. 5 Splits of 70 and 30 (a, b) confusion matrices, and (c, d) Graph of PR and ROC.

Table 3 and Figure 6 denote the DFU detection result of the ADFUDC-SAODL methodology with 70% and 30%. The solution represents that the ADFUDC-SAODL methodology properly identifies the occurrences. With 70%TRAP, the ADFUDC-SAODL algorithm presents an average $accur_y$, $preci_n$, $recal_l$, F_{score} and MCC of 94.00%, 94.00%, 94.00%, 94.00%, and 88.00%, respectively. Also, on 30%TESPH, the ADFUDC-SAODL method presents an average $accur_y$, $preci_n$, $recal_l$, F_{score} and MCC of 95.62%, 95.71%, 95.62%, 95.66%, and 91.33%, respectively.

Table 3. DFU detection outcome of the ADFUDC-SAODL system with 70% and 30%

Class	$Accur_y$	$Preci_n$	$Recal_l$	F_{score}	MCC
70% TRAPH					
Normal (Healthy)	94.19	93.64	94.19	93.91	88.00
Abnormal (DFU)	93.82	94.35	93.82	94.08	88.00
Average	**94.00**	**94.00**	**94.00**	**94.00**	**88.00**
30% TESPH					
Normal (Healthy)	96.79	94.97	96.79	95.87	91.33
Abnormal (DFU)	94.44	96.45	94.44	95.44	91.33
Average	**95.62**	**95.71**	**95.62**	**95.66**	**91.33**

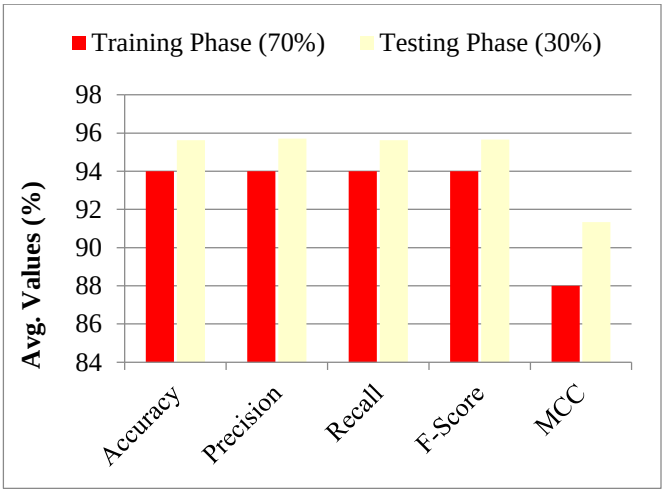

Fig. 6 Average of ADFUDC-SAODL method under 70%TRAPH and 30%TESPH

The comparison outcomes of the ADFUDC-SAODL methodology with recent algorithms are displayed in Table 4 and Figure 7 [29-31]. The stimulated outcome implied that the ADFUDC-SAODL system surpassed other models. In terms of $accur_y$, the ADFUDC-SAODL model has greater $accur_y$ of 97.57%, whereas the GoogLeNet, VGG16, AlexNet, DFINET, Inception ResNetV2, ResNet50, SqueezeNet, and EfficientNet models have lower $accur_y$ of 79.66%, 83.11%, 83.22%, 91.98%, 67.60%, 84.76%, 82.88%, and 93.90%, respectively.

Table 4. Comparison analysis of the ADFUDC-SAODL system with existing approaches

Classifier	$Accur_y$	$Preci_n$	$Recal_l$	F_{score}
GoogLeNet	79.66	73.58	92.54	81.98
VGG16 Model	83.11	85.74	81.45	83.54
AlexNet Classifier	83.22	78.65	91.19	84.46
DFINET Model	91.98	93.72	90.57	92.12
Inception ResNetV2	67.60	67.20	68.80	68.00
ResNet50 Technique	84.76	83.27	89.80	85.00
SqueezeNet Classifier	82.88	91.81	72.20	80.83
EfficientNet Model	93.90	92.80	93.20	93.11
ADFUDC-SAODL	97.57	97.47	97.57	97.5

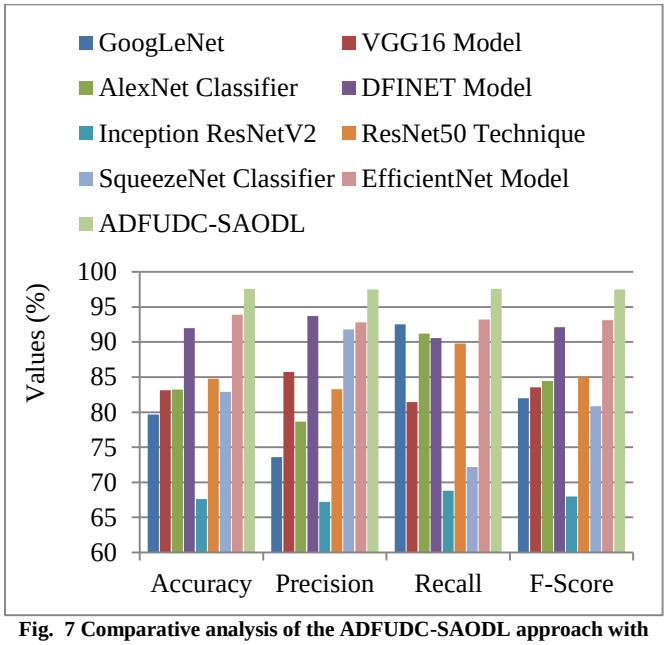

Fig. 7 Comparative analysis of the ADFUDC-SAODL approach with existing methods

Also, for $preci_n$, the ADFUDC-SAODL methodology has a greater $preci_n$ of 97.47% while the GoogLeNet, VGG16, AlexNet, DFINET, Inception ResNetV2, ResNet50, SqueezeNet, and EfficientNet models have a lower $preci_n$ of 73.58%, 85.74%, 78.65%, 93.72%, 67.20%, 83.27%, 91.81%, and 92.80%, respectively. Finally, according to F_{score}, the ADFUDC-SAODL approach contains a greater F_{score} of 97.5% while the GoogLeNet, VGG16, AlexNet, DFINET,

Inception ResNetV2, ResNet50, SqueezeNet, and EfficientNet models have a minimum F_{score} of 81.98%, 83.54%, 84.46%, 92.12%, 68.00%, 85.00%, 80.83%, and 93.11%. These results highlighted the betterment of the proposed model over other models on DFU detection and classification. The enhanced performance is due to the integration of the MResCaps-based feature extractor, CRNN-based classification, and SAO-based parameter tuning.

5. Conclusion

In this article, an innovative ADFUDC-SAODL model is proposed, which enables the detection and classification of DFU disease images. It comprises four distinct stages involving image pre-processing, MResCaps-based feature extractor, CRNN-based classification, and SAO-based parameter tuning. At first, the image pre-processing stage involves two levels, such as noise removal using the WF method and contrast enhancement using the CLAHE model. For the feature representation process, the MResCaps framework is exploited. Besides, the CRNN model is used for the classification of DFU. At last, the SAO method optimally tunes the parameters of the CRNN system by gaining enhanced results. An extensive set of simulations was involved to exhibit the encouraging outcomes of the ADFUDC-SAODL methodology. The stimulated outcomes implied the proficient performance of the ADFUDC-SAODL methodology across other recent models. Therefore, the ADFUDC-SAODL methodology is found to be a robust tool for automated DFU detection and classification process.

References

[1] Moi Hoon Yap et al., "Deep Learning in Diabetic Foot Ulcers Detection: A Comprehensive Evaluation," *Computers in Biology and Medicine*, vol. 135, pp. 1-17, 2021. [CrossRef] [Google Scholar] [Publisher Link]

[2] Angelo Argenteri et al., "History of the Diagnosis and Treatment of Critical Limb Ischemia and Diabetic Foot," *Seminars in Vascular Surgery*, vol. 31, no. 2-4, pp. 25-42, 2018. [CrossRef] [Google Scholar] [Publisher Link]

[3] James C. Stanley, and Andrew M. Collier, "The Diabetic Foot and Ankle," *Orthopedie Traumatologie*, vol. 23, no. 1, pp. 61-68, 2009. [CrossRef] [Google Scholar] [Publisher Link]

[4] William A Wood, and Michael A Wood, "Decompression of Peripheral Nerves for Diabetic Neuropathy in the Lower Extremity," *The Journal of Foot and Ankle Surgery*, vol. 42, no. 5, pp. 268-275, 2003. [CrossRef] [Google Scholar] [Publisher Link]

[5] Muhammad Adam et al., "Computer Aided Diagnosis of Diabetic Foot using Infrared Thermography: A Review," *Computers in Biology and Medicine*, vol. 91, pp. 326-336, 2017. [CrossRef] [Google Scholar] [Publisher Link]

[6] Rebecca M. Crocker et al., "Patient Perspectives on the Physical, Psycho-social, and Financial Impacts of Diabetic Foot Ulceration and Amputation," *Journal of Diabetes and its Complications*, vol. 35, no. 8, pp. 1-5, 2021. [CrossRef] [Google Scholar] [Publisher Link]

[7] Emmanuel Navarro-Floresor, and Omar Cauli, "Quality of Life in Individuals with Diabetic Foot Syndrome," *Endocrine Metabolic & Immune Disorders - Drug Targets*, vol. 20, no. 9, pp. 1365-1372, 2020. [CrossRef] [Google Scholar] [Publisher Link]

[8] S. A. Bus et al., "IWGDF Guidance on the Prevention of Foot Ulcers in at-risk Patients with Diabetes," *Diabetes/Metabolism Research and Reviews*, vol. 32, no. S1, pp. 16-24, 2016. [CrossRef] [Google Scholar] [Publisher Link]

[9] Pouya Saeedi et al., "Global and Regional Diabetes Prevalence Estimates for 2019 and Projections for 2030 and 2045: Results from the International Diabetes Federation Diabetes Atlas, 9th edition," *Diabetes Research and Clinical Practice*, vol. 157, pp. 1-10, 2019. [CrossRef] [Google Scholar] [Publisher Link]

[10] Manu Goyal et al., "Recognition of Ischaemia and Infection in Diabetic Foot Ulcers: Dataset and Techniques," *Computers in Biology and Medicine*, vol. 117, pp. 1-10, 2020. [CrossRef] [Google Scholar] [Publisher Link]

[11] S. V. N. Murthy et al., "Automated Detection of Infection in Diabetic Foot Ulcer Using Pre-trained Fast Convolutional Neural Network with U++Net," *SN Computer Science*, vol. 5, 2024. [CrossRef] [Google Scholar] [Publisher Link]

[12] Mohammad H. Alshayeji, Silpa ChandraBhasi Sindhu, and Sa'ed Abed, "Early Detection of Diabetic Foot Ulcers from Thermal Images using the Bag of Features Technique," *Biomedical Signal Processing and Control*, vol. 79, 2023. [CrossRef] [Google Scholar] [Publisher Link]

[13] T. Arumuga Maria Devi, and R. Hepzibai, "Diabetic Foot Ulcer Classification of Hybrid Convolutional Neural Network on Hyperspectral Imaging," *Multimedia Tools and Applications*, vol. 83, pp. 55199-55218, 2024. [CrossRef] [Google Scholar] [Publisher Link]

[14] Sunnam Nagaraju et al., "Automated Diabetic Foot Ulcer Detection and Classification Using Deep Learning," *IEEE Access*, vol. 11, pp. 127578-127588, 2023. [CrossRef] [Google Scholar] [Publisher Link]

[15] Sujit Kumar Das, Suyel Namasudra, and Arun Kumar Sangaiah, "HCNNet: Hybrid Convolution Neural Network for Automatic Identification of Ischaemia in Diabetic Foot Ulcer Wounds," *Multimedia Systems*, vol. 30, 2024. [CrossRef] [Google Scholar] [Publisher Link]

[16] Sujit Kumar Das et al., "AESPNet: Attention Enhanced Stacked Parallel Network to Improve Automatic Diabetic Foot Ulcer Identification," *Image and Vision Computing*, vol. 138, 2023. [CrossRef] [Google Scholar] [Publisher Link]

[17] Nouf F. Almufadi, Haifa F. Alhasson, and Shuaa S. Alharbi, "E-DFu-Net: An Efficient Deep Convolutional Neural Network Models for Diabetic Foot Ulcer Classification," *Biomolecules and Biomedicine*, vol. 25, no. 2, pp. 445-460, 2026. [CrossRef] [Google Scholar] [Publisher Link]

[18] Abdul Rahaman Wahab Sait, and Ramprasad Nagaraj, "Diabetic Foot Ulcers Detection Model Using a Hybrid Convolutional Neural Networks–Vision Transformers," *Diagnostics*, vol. 15, no. 6, pp. 1-22, 2025. [CrossRef] [Google Scholar] [Publisher Link]

[19] Pramod Singh Rathore et al., "A Feature Explainability-based Deep Learning Technique for Diabetic Foot Ulcer Identification," *Scientific Reports*, vol. 15, pp. 1-21, 2025. [CrossRef] [Google Scholar] [Publisher Link]

[20] Raj Kumar Gudivaka et al., "Diabetic Foot Ulcer Classification Assessment Employing an Improved Machine Learning Algorithm," *Technology and Health Care*, vol. 33, no. 4, pp.1645-1660, 2025. [CrossRef] [Google Scholar] [Publisher Link]

[21] Md ZakirHossain et al., "Advanced Classification of Diabetic Foot Ulcers Using Custom and Deep Learning Models," *2025 IEEE International Conference on Emerging Technologies and Applications (MPSec ICETA)*, Gwalior, India, pp. 1-6, 2025. [CrossRef] [Google Scholar] [Publisher Link]

[22] Saswati Debnath et al., "Sustainable AI for Diabetic Foot Ulcer Detection: A Deep Learning Approach for Early Diagnosis," *Discover Applied Sciences*, vol. 7, pp. 1-21, 2025. [CrossRef] [Google Scholar] [Publisher Link]

[23] P. Abirami, and S.N.S. Rajini, "Detection of Tuberculosis Using Optimized Deep Learning Approach with Enhanced Selective Median (ESMF) Filter," *African Journal of Biological Sciences*, vol. 6, no. 2, pp. 193-210, 2024. [Google Scholar]

[24] Ahmed Naser, "A Proposed CLCOA Technique based on CLAHE using Cat Optimized Algorithm for Plants Images Enhancement," *Wasit Journal of Computer and Mathematics Science*, vol. 3, no. 1, pp. 18-27, 2024. [Google Scholar]

[25] Sümeyra Büşra Şengül, and İlker Ali Özkan, "MResCaps: Enhancing Capsule Networks with Parallel Lanes and Residual Blocks for High-performance Medical Image Classification," *International Journal of Imaging Systems and Technology*, vol. 34, no. 4, pp. 1-16, 2024. [CrossRef] [Google Scholar] [Publisher Link]

[26] Bing-Rui Chen et al., "Real-time Arrival Picking of Rock Microfracture Signals based on Convolutional-recurrent Neural Network and its Engineering Application," *Journal of Rock Mechanics and Geotechnical Engineering*, vol. 16, no. 3, pp. 761-777, 2024. [CrossRef] [Google Scholar] [Publisher Link]

[27] Jinyi Xie et al., "An Enhanced Snow Ablation Optimizer for UAV Swarm Path Planning and Engineering Design Problems," *Heliyon*, vol. 10, no. 18, pp. 1-18, 2024 [CrossRef] [Google Scholar] [Publisher Link]

[28] Diabetic Foot Ulcer (DFU). [Online]. Available: https://www.kaggle.com/datasets/laithjj/diabetic-foot-ulcer-dfu

[29] J. Yogapriya et al., "Automated Detection of Infection in Diabetic Foot Ulcer Images Using Convolutional Neural Network," *Journal of Healthcare Engineering*, vol. 2022, pp. 1-12, 2022. [CrossRef] [Google Scholar] [Publisher Link]

[30] Mehnoor Ahsan et al., "A Deep Learning Approach for Diabetic Foot Ulcer Classification and Recognition," *Information*, vol. 14, no. 1, pp. 1-10, 2023. [CrossRef] [Google Scholar] [Publisher Link]

[31] Puneeth N. Thotad et al., "Diabetic Foot Ulcer Detection using Deep Learning Approaches," *Sensors International*, vol. 4, pp. 1-9, 2023. [CrossRef] [Google Scholar] [Publisher Link]